

Storage properties of a quantum perceptron

Katerina Gratsea ^{1,*}, Valentin Kasper,¹ and Maciej Lewenstein ^{1,2}

¹*ICFO-Institut de Ciències Fotòniques, The Barcelona Institute of Science and Technology, Av. Carl Friedrich Gauss 3, 08860 Castelldefels (Barcelona), Spain*

²*ICREA, Pg. Lluís Companys 23, 08010 Barcelona, Spain*



(Received 18 December 2022; revised 7 March 2024; accepted 18 April 2024; published 20 August 2024)

Driven by growing computational power and algorithmic developments, machine learning methods have become valuable tools for analyzing vast amounts of data. Simultaneously, the fast technological progress of quantum information processing suggests employing quantum hardware for machine learning purposes. Recent works discuss different architectures of quantum perceptrons, but the abilities of such quantum devices remain debated. Here, we investigate the storage capacity of a particular quantum perceptron architecture by using statistical mechanics techniques and connect our analysis to the theory of classical spin glasses. Specifically, we focus on one concrete quantum perceptron model and explore its storage properties in the limit of a large number of inputs.

DOI: [10.1103/PhysRevE.110.024127](https://doi.org/10.1103/PhysRevE.110.024127)

I. INTRODUCTION

The rapid development of machine learning algorithms revolutionized our day-to-day lives and created novel connections between such diverse fields as computer science and neuroscience [1], physics [2], and engineering [3]. At the core of the success of machine learning are deep classical neural networks [4]. Whereas classical neural networks initially had a biological motivation [5], the modern perspective considers classical neural networks as a form of information processing [6–9]. The building block of these networks is the neuron or perceptron as it was initially introduced by Rosenblatt and understanding its properties is still an active research direction [2,10].

Nowadays, with the advent of quantum technologies even the simple quantum analogs of classical perceptrons referred to this work as quantum perceptrons are back in the center of interests, due to their possible realizations with ultracold atoms, trapped ions, Rydberg atoms, superconducting qubits, or photonic systems (cf. [11]). This essentially opens the road for implementing machine learning concepts directly on quantum hardware [12,13] and potentially leveraging quantum mechanics for efficient information processing.

Contrary to the classical perceptron where each physical spin encodes a classical bit, different encodings could be used for the quantum perceptron [14]. For example, the straightforward realization is following the standard mapping where each classical spin is promoted to quantum spin- $\frac{1}{2}$ Pauli operator [15]. Another approach is the binary encoding where the binary string values of the classical spins (i.e., 101) corresponds to the computational basis states (i.e., $|101\rangle$) of the wave function of the quantum system [16]. Also, the string values of the classical spins could be mapped to the

amplitudes of the computational basis states of the wave function which is referred to as amplitude encoding [17].

Throughout this work we focus on amplitude encoding of information which has a clear efficiency of the memory resources used since for N classical spins only $\log_2(N)$ are needed. But the properties of such perceptron models as general learning machines are still an open question. To this end, we aim to bridge the gap between quantum computation and learning theory by applying statistical physics techniques as used to explore the properties of classical perceptron models as well [18]. One advantage of statistical physics is the computation of global properties of physical systems without knowing the microscopic details.

One important application of statistical physics to information processing concerns the storage capacity of perceptrons and neural networks [19,20] which corresponds to the models' ability to obtain the desired input-output relations given a choice on the learning rules [21]. Gardner in her seminal works [22,23] addressed the challenge of analyzing the properties of such models without specifying the learning rule, which is usually referred to as Gardner's program. The work of Gardner is of significant historical importance but also sheds light on the most important questions of artificial networks and perceptrons as general learning machines.

Moreover, Gardner's program is extremely general, adaptive, and versatile and has already been applied to different quantum information problems, such as various models of quantum perceptrons, quantum neural networks (NN), and more. For example, Gardner's program inspired investigation of the relative volume of parent Hamiltonians having a target ground state up to some fixed error ϵ [24]. Moreover, Gardner's relative volume approach clearly inspired the pioneering attempts to estimate the volume of quantum correlated states, such as entangled states [25], where integration is over the unitary group in a very high dimension. In Ref. [26] a quantum perceptron is defined as a unitary map followed

*Contact author: gratsea.katerina@gmail.com

by projective measurements in a multidimensional Hilbert space, where the calculation of the relative volume reduces to the calculation of the volume in the unitary group space. Recently, Gardner's program has been used on quantum neural network (QNN) models [27] corresponding to completely positive trace-preserving maps (CPTP), where the relative volume requires integration over the space of maps.

In this work, we apply Gardner's program to a specific quantum analog of the classical perceptron introduced in [17] to explore its storage capacity. This quantum perceptron model has a direct implementation on quantum hardware [17] and uses amplitude encoding which is beneficial in terms of memory resources as mentioned earlier. But, for this perceptron model it is not clear how the storage capacity will compare to its classical counterpart contrary to the quantum perceptron models [15,28], which have the same storage capacity. Therefore, we aim to perform a reasonable comparison of the maximum storage capacity of this quantum perceptron model with its classical counterpart. This work brings us one step closer to understanding whether they provide hope for quantum advantage and sheds light on the most important questions of contemporary quantum machine learning models as general learning machines [29].

This article is structured as follows: After motivating Gardner's program in this section, we discuss Gardner's program in detail and apply it to a quantum perceptron architecture in Sec. II. In Sec. III, we discuss the main result: the calculation of the storage capacity of a quantum perceptron by applying statistical physics techniques. Finally, we give the computational details of Gardner's program for the quantum perceptron in Sec. IV.

II. QUANTUM PERCEPTRONS AND GARDNER'S PROGRAM

A. Classical perceptron model

A classical perceptron is a function that maps an N -dimensional input $\vec{i}^\mu = (i_1^\mu, \dots, i_N^\mu)^T$ of length \sqrt{N} onto an output σ^μ , where the weight vector $\vec{w} = (w_1, \dots, w_N)^T$, also of length \sqrt{N} determines the information processing. The additional label $\mu \in \{1, 2, \dots, p\}$ denotes different pairs of input vectors and outputs [6,18]. Moreover, we consider the activation function

$$\sigma^\mu = \theta(\vec{i}^\mu \cdot \vec{w} / \sqrt{N} - \kappa), \quad (1)$$

so that for the stored pattern vectors \vec{i}^μ , their scalar product with the weight vector \vec{w} must be positive. Here, $\theta(\cdot)$ is the Heaviside function realizing the nonlinearity of the perceptron model [see Fig. 1(a)]. Following Gardner, we introduce the threshold κ that measures how robust and stable are the stored patterns. Note that storage capacity of the perceptron (see below) must decrease with κ , the relative volume of perceptrons that fulfill Eq. (1) must shrink. Note also that at $\kappa \rightarrow 0$ the relative volume does not diverge, but rather goes to a finite value. Here we would like also to emphasize that there are different options for the input and weight vectors, i.e., binary, continuous, Gaussian, etc., and at each section we specify which case we are considering.

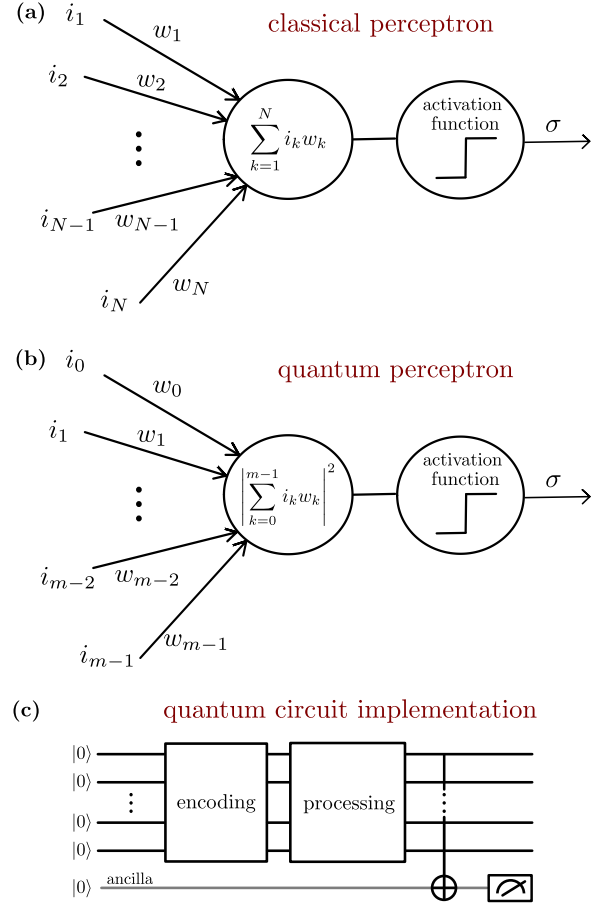


FIG. 1. Classical and quantum perceptrons. (a) Schematic outline of the classical perceptron: an N -dimensional input array \vec{i} is processed with a weight vector \vec{w} such that $\vec{i} \cdot \vec{w}$ enters the activation function. (b) Schematic outline of the quantum perceptron: an m -dimensional input array \vec{i} is processed with a weight vector \vec{w} to produce the inner product squared of these vectors. Both cases, the classical and the quantum, employ a nonlinear activation leading to the output σ . (c) Quantum circuit implementation of the quantum perceptron following the work of Tacchino *et al.* [17]. An encoding unitary realizes the input state $|\psi_{\vec{i}}\rangle$ and the processing unitary computes the inner product of the input and weight vectors. The outcome is then written on the ancilla qubit with a multi-controlled-NOT gate. Finally, the activation is measured by the readout of the ancilla qubit.

B. Quantum perceptron model

A quantum analog of the classical perceptron [17] is depicted in Fig. 1(b) with the corresponding quantum circuit in Fig. 1(c). In this quantum perceptron the connection between the inputs, outputs, and weights is given by the activation function

$$\sigma^\mu = \theta\left(\frac{1}{m}|\vec{i}^\mu \cdot \vec{w}|^2 - \kappa\right), \quad (2)$$

where the nonlinearity of the perceptron is realized by the measurement [see Fig. 1(b)].

In the quantum case the input vector is $\vec{i}^\mu = (i_0^\mu, \dots, i_{m-1}^\mu)^T$ and the weight vector is $\vec{w} = (w_0, \dots, w_{m-1})^T$, both of length \sqrt{m} , where m is the dimension of the Hilbert

space. The vectors \vec{i}^μ and \vec{w} are encoded in normalized quantum states

$$|\psi_{\vec{i}}\rangle = \frac{1}{\sqrt{m}} \sum_{j=0}^{m-1} i_j |j\rangle, \quad (3a)$$

$$|\phi_{\vec{w}}\rangle = \frac{1}{\sqrt{m}} \sum_{j=0}^{m-1} w_j |j\rangle, \quad (3b)$$

respectively, with the orthonormal basis vectors $|j\rangle$ form the computational basis and we focused on the case of binary inputs and weights. The encoding unitary $U_{\vec{i}}$ prepares the input state, while the processing unitary $V_{\vec{w}}$ computes the inner product between \vec{i} and \vec{w} . The precise definition of the unitaries can be found in Appendix A.

C. Activation functions

It is important to discuss the differences between the classical activation function and the quantum (i.e., quadratic) activation function. In the classical case, the perceptron is a linear classifier, and its activation function depends linearly on the weighted signal. In general, the quadratic activation function introduces a nonlinearity to the model. We refer here to Ref. [30], where the concept of a quadratic activation function has already been discussed.

In general, according to Ref. [30], quadratic or, more generally, nonlinear activation function might improve or deteriorate the performance of the classical perceptron. In fact, recent works have explored a quadratic activation function of a classical neuron. Even though their increased representation and efficiency [31], they have increased computational costs and restricted expressive abilities [32]. Regarding the storage capacity, the authors in the work of [32] discuss that a two-layer neural network with N inputs, K hidden units, binary outputs, and a quadratic activation function results in the same value of the storage capacity with the quantum perceptron. Moreover, taking into account that $\alpha_{c,\max}$ has a finite value for the quantum perceptron and that m equals the dimension of the Hilbert space ($m = 2^N$), the number of patterns that can be stored is exponential in the number of spins N in agreement with recent works [33–35]. For example, in the recent work [27] the authors applied Gardner’s program to attractor quantum neural networks and found that the learning of P patterns at the order of $2^{N/2}$ is possible.

The same quadratic activation function that we use for quantum perceptron can be directly implemented in a classical perceptron, but it does not seem to make a lot of sense. Our activation function is directly related to quantum measurement theory: it estimates how much a given set of normalized weights can be similar (in the sense of the squared scalar product) to a random pattern. This is in principle a geometrical question and can be considered in a purely classical system, but it is not the true goal for introducing nonlinear activation functions.

At this stage it is worth evoking our recent work [36], where we prove that regularized restricted Boltzmann machines (RBM) can store the exponential number of patterns, as large as 2^V , where V is the number of visible neurons. These properties resemble dense associative memory

networks or modern Hopfield networks [37–40]. Indeed, if one would marginalize an RBM over its hidden neurons, the result would be a network consisting only of V visible neurons with multispin interactions, and nonlinear activation function in the spirit of Refs. [38,41], and the classical book [30]. Would one marginalize a regularized RBM over hidden neurons, the resulting network, at low temperatures, can have the exponential capacity for storage and perfect retrieval of arbitrarily correlated patterns. In this sense, BMs with regularized weights are related to the embeddings of dense associative memory networks in a set of two-body interaction models [39].

D. Gardner’s program

The correct choice of the weights results in a desired input-output relation, i.e., a specific mapping between the input \vec{i}^μ and the output σ^μ . A learning rule is usually applied to find the correct weights, such as the Hebbian rule [42]. While the Hebbian rule has an appealing simplicity, Gardner, in her works [22,23], was interested in the global properties of the classical perceptron model without specifying the learning rule. She asked the following question: What is the maximum number of input-output patterns that the classical perceptron can realize? Therefore, she considered the relative volume in the space of possible weights, which realizes a given input-output relation.

E. Storage capacity

The problem of storage capacity goes indeed back to the theory of classical perceptrons [43]. In the “classic” paper from 1964 [44], Cover demonstrated using simple geometrical arguments that the separating capacities of families of nonlinear decision surfaces by a direct application of a theorem in classical combinatorial geometry. It is shown that a family of surfaces having N degrees of freedom has a natural separating capacity of $2N$ pattern vectors, thus extending and unifying earlier results of others on the pattern-separating capacity of hyperplanes. Thus, the critical storage capacity of a classical perceptron is $\alpha_c = 2$.

The problem of storage capacity returned in 1982 in the seminal paper of Hopfield [19], who has shown numerically that the Hopfield model with the, so-called, Hebbian learning rule may store $0.14N$ random patterns. Gardner came back to the problem analyzing the shrinking in the volume of perceptrons that correctly reproduce the desired input-output relations normalized to the volume of connection vectors \vec{w} . The advantage of the work of Gardner was that it calculated storage capacity independently of the learning rule used. It also reproduced correctly the classical geometrical bound of Cover [44].

Following Gardner’s work, the storage capacity can be obtained from the fraction of \vec{w} space which *correctly* and *exactly* reproduces the desired input-output relations normalized to the volume of vectors \vec{w} . When increasing the number of patterns, the volume of vectors \vec{w} typically shrinks, and the relative volume of the weights vanishes. The limit of vanishing relative volume defines the storage capacity of the perceptron [18].

From the definition of the storage capacity, the difference between the classical and quantum perceptrons results from two aspects of to the definition of quantum perceptron proposed in [17]. The classical perceptron checks whether the signal corresponding to a given input pattern has an appropriate sign at the output. Quantum perceptron uses quantum measurement principles, and checks for a given input pattern how big are the quantum overlaps of output states. Quantum perceptron by definition does not reproduce the input patterns *correctly* and *exactly*; it does it with certain optimal error, or better to say accuracy.

The other important aspect is that of the different dimensionality of the input vectors, which equals N physical inputs for the classical perceptron. In contrast, in the quantum case, the number of inputs equals the dimension of the Hilbert space m . Hence, for the classical perceptron we have $\alpha_c = p/N$ (i.e., the capacity p is proportional to the number of spins N), while for the quantum perceptron $\alpha_c = p/m$ (i.e., the capacity is exponential in the number of spin configurations, $p \propto m = 2^N$). For the classical perceptron, the storage capacity is known to be 2 (for $\kappa = 0$) and was calculated, for example, in [18,22,23,30,44]. More, precisely in the classical perceptron, when $\alpha > \alpha_c(\kappa)$, the relative volume shrinks abruptly to zero. In contrast, when $\alpha \leq \alpha_c(\kappa)$, the relative volume is nonzero but shrinks moderately slowly exponentially with m .

It is rather difficult to compare this situation with our results obtained for the quantum perceptron. First of all, critical capacity and the nature of the phase transition depend on the form of weights we use (spherical weights, Gaussian distributed inputs, Ising weights and inputs). For various cases, capacity ranges between more than 13 and 0.125, but as noted above it corresponds to recognition intrinsically associated with quantum measurement errors.

Finally, we would like to mention parameter κ , introduced by Gardner in her original paper [22]. While strictly speaking, the classical perceptron checks whether the signal corresponding to a given input pattern has an appropriate (say positive) sign at the output, in principle one can demand that the signal is greater than a certain parameter κ . In the case of classical perceptrons with the scaling of connections proposed by Gardner, κ is N independent. In the more complex quantum case, we need to scale κ appropriately as in Eq. (2), and as discussed in the next section.

F. Calculation of the relative volume

In the following, we will focus on quantum perceptrons. The abundance of weights, which leads to desired input-output relations, can be treated by averaging over the weight vectors \vec{w} . This averaging gives rise to an ensemble of quantum machines, which can be analyzed with statistical physics tools. To define a finite volume of weights [23] we constrain the weight vector \vec{w} . Similar to Gardner's work one can consider two types of constraints: spherical weights, i.e., $|\vec{w}|^2 = m$, and Ising weights $w_i = \pm 1$. The corresponding integration measures [30] are

$$\rho_S[\vec{w}] = \frac{1}{V_{S_0}} \delta(|\vec{w}|^2 - m), \quad (4a)$$

$$\rho_I[\vec{w}] = \frac{1}{V_{I_0}} \prod_k [\delta(w_k - 1) + \delta(w_k + 1)] \quad (4b)$$

with the normalization (see Appendix B)

$$V_{S_0} = \int_w \delta(|\vec{w}|^2 - m), \quad (5a)$$

$$V_{I_0} = \int_w \prod_k [\delta(w_k - 1) + \delta(w_k + 1)]. \quad (5b)$$

Then the relative volume of perceptrons, which fulfill a specific input-output relation, is given by

$$V_M = \int_w \prod_\mu \theta\left(\frac{1}{m} |\vec{i}^\mu \cdot \vec{w}|^2 - \kappa\right) \rho_M[\vec{w}], \quad (6)$$

where the label $M = S$ for the spherical constraint or $M = I$ for the Ising constraint. The threshold κ takes values in $[0, m]$ and in the limit $\kappa \rightarrow 0$ the relative volume allows us to obtain the maximum storage capacity of the quantum perceptron model [18,30]. We calculate the relative volume using the integral representation of the Heaviside function

$$\theta(y - \kappa) = \int_\kappa^\infty d\lambda \int_{-\infty}^\infty \frac{dx}{2\pi} e^{ix(\lambda - y)}, \quad (7)$$

which we insert into Eq. (6). In the following we outline the calculation of the relative volume for the case of spherical weights and present the details of the calculation in Sec. IV.

1. Spherical weights

The distribution of the spherical weights is given in Eq. (4a) and contains a delta function, which we represent via

$$\delta(|\vec{w}|^2 - m) = \int_{-\infty}^\infty \frac{dE}{2\pi} e^{iE(|\vec{w}|^2 - m)}. \quad (8)$$

Further, we average over the input vector \vec{i}^μ to avoid bias towards specific input vectors. The average with respect to \vec{i}^μ is denoted as $\langle\langle \cdot \rangle\rangle$. The expression for the relative volume becomes

$$\begin{aligned} \langle\langle V_S \rangle\rangle &= \frac{1}{V_{S_0}} \int_w \int_\lambda \int_x \int_E \exp[iE(|\vec{w}|^2 - m)] \\ &\times \left\langle\left\langle \exp\left[i \sum_\mu x^\mu \left(\lambda^\mu - \frac{1}{m} |\vec{i}^\mu \cdot \vec{w}|^2\right)\right] \right\rangle\right\rangle, \quad (9) \end{aligned}$$

where the integration measure is given in Appendix B.

Similar to Gardner we make the observation that Eq. (9) is a partition function of a classical spin glass, where $\langle\langle \cdot \rangle\rangle$ is interpreted as a disorder average and \vec{w} is a classical spin variable. As for classical spin glasses [18,30] we calculate $\langle\langle \ln V_S \rangle\rangle$ via the replica trick

$$\langle\langle \ln V_S \rangle\rangle = \lim_{n \rightarrow 0} \frac{\langle\langle V_S^n \rangle\rangle - 1}{n}, \quad (10)$$

which leads to the replicated variables \vec{w}^α , x^α , λ^α with the replica index $\alpha \in \{1, \dots, n\}$. Following the notation introduced in [18], we would like to emphasize that the reader should not confuse the storage capacity α with the replica index. In addition, we introduce the spin glass order parameter

$q^{\alpha\beta}$ and its conjugate $F^{\alpha\beta}$ via the integral

$$\begin{aligned} 1 &= \int_{-\infty}^{\infty} dq^{\alpha\beta} \delta\left(q^{\alpha\beta} - \frac{1}{m} \sum_k w_k^\alpha w_k^\beta\right) \\ &= m \int_{-\infty}^{\infty} dq^{\alpha\beta} \int_{-\infty}^{\infty} \frac{dF^{\alpha\beta}}{2\pi} e^{imF^{\alpha\beta}(q^{\alpha\beta} - \frac{1}{m} \sum_k w_k^\alpha w_k^\beta)} \end{aligned} \quad (11)$$

with $\alpha < \beta$. This identity is also referred to as Hubbard-Stratonovich transformation (see [45,46] for details).

Ising inputs. Here we assume that Ising inputs $i_k^\mu = \pm 1$. In the next step, we perform the average over the inputs and assume small fluctuations of x^α , which leads to

$$\langle\langle V_S^n \rangle\rangle = \frac{1}{V_{S_0}^n} \int_F \int_q \int_E e^{mG}, \quad (12)$$

with integration measure given in Appendix B and where we introduced the effective potential

$$G = \alpha G_1[q^{\alpha\beta}] + G_2[E^\alpha, F^{\alpha\beta}] - i \sum_\alpha E^\alpha + i \sum_{\alpha < \beta} F^{\alpha\beta} q^{\alpha\beta} \quad (13)$$

with the storage capacity α and the two contributions

$$\begin{aligned} G_1[q^{\alpha\beta}] &= \ln \int_{-\infty}^{\infty} \prod_\alpha \frac{dx^\alpha}{2\pi} \int_\kappa \prod_\alpha d\lambda^\alpha \\ &\times \exp\left(i \sum_\alpha x^\alpha (\lambda^\alpha - 1) - \sum_\alpha (x^\alpha)^2 \right. \\ &\left. - 2 \sum_{\alpha < \beta} (q^{\alpha\beta})^2 x^\alpha x^\beta\right) \end{aligned} \quad (14)$$

and

$$\begin{aligned} G_2[E^\alpha, F^{\alpha\beta}] &= \ln \int_{-\infty}^{\infty} \prod_\alpha dw^\alpha \\ &\times \exp\left(i \sum_\alpha E^\alpha (w^\alpha)^2 - i \sum_{\alpha < \beta} F^{\alpha\beta} w^\alpha w^\beta\right). \end{aligned} \quad (15)$$

Comparing the integrals for the effective potential reveals a quadratic dependency on $q^{\alpha\beta}$ for the quantum model and a linear dependence on $q^{\alpha\beta}$ for the classical model within the exponents. The nonlinear dependence in the quantum case is a consequence of the measuring process, which involves the modulus square.

Note that $G = G(F, E, q; \alpha, \kappa)$ is a function of integration variables, and depends parametrically on α and κ . The integral over F, E, q in Eq. (13) can be evaluated using the saddle point method, due to the exponential dependence on m . In the replica symmetric case, one can eliminate dependence on E, F , so that the effective potential or free energy of interest can be defined in the limit n going to zero,

$$g(q; \alpha, \kappa) = \lim_{n \rightarrow 0} \frac{1}{n} G(q; \alpha, \kappa). \quad (16)$$

It is useful also to introduce the proper normalization for the saddle point value of the effective potential, coming from

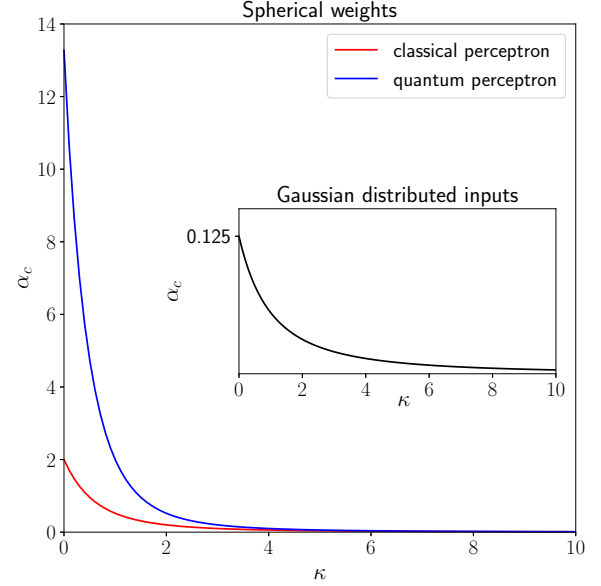


FIG. 2. Storage properties of perceptrons for spherical weights: storage capacity for the classical (red line with maximum value at 2) and quantum (blue line with maximum value at 13.27) perceptrons as a function of the threshold κ with Ising inputs. For $\kappa = 0$, the storage capacity has a maximum, whereas the storage capacity decays for $\kappa \gg 0$. In the inset, we plot the critical storage capacity as a function of κ for spherical weights, but with Gaussian distributed inputs.

subtracting the logarithm of $n \ln(V_{S_0})$:

$$\tilde{g}(q_s; \alpha, \kappa) = g(q_s; \alpha, \kappa) - g(q_s; \alpha, \kappa = 0). \quad (17)$$

This quantity is strictly nonpositive. If \tilde{g} is one, then the volume is one (as it should happen for $\kappa = 0$). If \tilde{g} is $-\infty$, then the volume shrinks to zero (as it should happen for $\alpha > \alpha_c$). This may happen even for $\kappa = 0$, due to the approximate character of our calculations. Finally, when $0 > \tilde{g} > -\infty$, the relative volume decreases exponentially with m as $\exp(m\tilde{g})$.

After the Hubbard-Stratonovich transformation we perform a saddle point approximation for large m and assume replica symmetry, which assumes that the replicas are statistically equivalent [47], i.e.,

$$q^{\alpha\beta} = q, \quad F^{\alpha\beta} = F, \quad E^\alpha = E. \quad (18)$$

The saddle point equations are

$$\frac{\partial G}{\partial E} = \frac{\partial G}{\partial F} = \frac{\partial G}{\partial q} = 0, \quad (19)$$

which we solve and subsequently perform the limit $n \rightarrow 0$. Taking the derivative of G with respect to q and analyzing the limit $q \rightarrow 1$, we observe that it leads to the saddle point solution for q is $q = 0$ for $\alpha \leq \alpha_c(\kappa)$ to the maximum critical storage capacity at $\kappa = 0$ of

$$\alpha_{c,\max} = 13.27 \geq 2. \quad (20)$$

In contrast, for $\alpha > \alpha_c(\kappa)$, q at the minimum of the effective potential becomes equal to 1, and the volume abruptly shrinks to zero. The saddle point approximation allows us to study the critical storage capacity $\alpha_c(\kappa)$ as a function of the threshold κ , which we depict in Fig. 2. Note, the phase transition has here

similar nature as in the classical perceptron. For $\alpha \leq \alpha_c(\kappa)$, the relative volume is equal to 1 for $\kappa = 0$. For $\kappa > 0$, the effective potential $\tilde{g} < 0$, and the volume shrinks moderately slowly exponentially with m as $\exp(m\tilde{g})$. For $\alpha > \alpha_c(\kappa)$, $\tilde{g} = -\infty$, and the volume is strictly equal to zero (for details see Methods section).

Gaussian distributed inputs. In this section, we discuss the case of inputs distributed according to a Gaussian normal distribution. The weights in turn are distributed according to Eq. (4a). We apply the replica trick (10), introduce the order parameters as in Eq. (11), and average over the inputs to calculate the effective potential G . A comparison to Eq. (12) reveals that only the expression for G_1 changes

$$G_1[q^{\alpha\beta}] = \ln \int_{-\infty}^{\infty} \prod_{\alpha} \frac{d\lambda^{\alpha}}{2\pi} \int_{\kappa}^{\infty} \prod_{\alpha} d\lambda^{\alpha} \times \exp \left[i \sum_{\alpha} x^{\alpha} \lambda^{\alpha} - \ln \det(1 + 2i\hat{A}) \right], \quad (21)$$

where we introduce the matrix A later in Eq. (48). Next, we assume replica symmetry, i.e.,

$$q^{\alpha\beta} = q, F^{\alpha\beta} = iF, \quad (22)$$

where the imaginary unit i is used to ensure that the saddle point solutions are real. Then the saddle point equations are

$$\frac{\partial G}{\partial F} = \frac{\partial G}{\partial q} = 0, \quad (23)$$

which we solve and subsequently perform the limit $n \rightarrow 0$. The saddle point equation given by the derivative with respect to q leads to

$$\alpha(2 + \kappa)^2 q = \frac{q}{2(1 - q)^2}. \quad (24)$$

This equation has one trivial solution $q = 0$ and one nontrivial in $0 < q < 1$. The nontrivial solution exists if and only if

$$2\alpha(2 + \kappa)^2 \geq 1. \quad (25)$$

For $\alpha \leq \alpha_c = (\frac{1}{2})(2 + \kappa)^2$ the solution is trivial, and the logarithm of the relative volume is close to zero, it is proportional to $\tilde{g} = -\alpha\kappa/2$, and for $\kappa = 0$ the volume is equal to one, while for $\kappa > 0$ it decreases exponentially as $\exp(m\tilde{g})$. Above α_c , the saddle point solution for q is nonzero, and the volume shrinks also exponentially with m , but much faster (for details see Methods section). We plot α_c in Fig. 2 for different values of κ and observe $\alpha_c \rightarrow \frac{1}{8}$ for $\kappa = 0$. The phase transition has a different character in comparison to Gardner's work [22]. In her work, the volume decreases exponentially with m below the critical α_c (where $q < 1$), and strictly shrinks to zero above the critical α_c (where $q = 1$). In our work, the volume is close to one below α_c (although it decreases slowly exponentially with m), and it starts to decrease much more rapidly exponentially with m above α_c . This is the result of the approximations used (expansion in q). In Appendix D we speculate how one could restore the ‘‘Gardner's nature’’ of the phase transition in our model with Gaussian inputs.

2. Ising weights and inputs

In the classical case the Ising weights were treated, for example, in [18,23,30]. Here, we use the Ising weights for the quantum case and employ Eqs. (4b) and (5) for the integration measure and normalization of the volume, respectively. We apply the replica trick (10), introduce the order parameters (11), and average over the inputs to calculate the effective potential. The contribution G_1 is the same as Eq. (15), while G_2 becomes

$$G_2[F^{\alpha\beta}] = \ln \sum_{\{w^{\alpha} = \pm 1\}} \exp \left(\sum_{\alpha < \beta} F^{\alpha\beta} w^{\alpha} w^{\beta} \right). \quad (26)$$

We assume replica symmetry [see Eq. (22)] and the saddle point equations [see Eq. (23)]. Solving the saddle point equations in the limit for $q \rightarrow 1$ we conclude that the storage capacity is

$$\alpha_c(\kappa) = \frac{4}{\pi} \left[\int_{-\kappa}^{\infty} Dy (\kappa + y)^2 \right]^{-1}, \quad (27)$$

where we used the abbreviation

$$\int_{-\infty}^{\infty} Dy = \sqrt{\frac{1}{2\pi}} \int_{-\infty}^{\infty} dy e^{-\frac{y^2}{2}}. \quad (28)$$

We would like to emphasize that the limit $\kappa \rightarrow 0$ gives the maximum storage capacity for the quantum perceptron model we are considering given its specific hardware implementation. At the limit $\kappa \rightarrow 0$ we are including all the patterns that could be activated, i.e., give a nonzero probability outcome [17]. This results to the maximal value of $\alpha_c(0) = 8/\pi$. In addition, we present the results of a Monte Carlo simulation in Fig. 3, which shows that as $m \rightarrow \infty$ and $\kappa \rightarrow 0$, the storage capacity is 3.55 ± 0.01 (see Appendix C for details). We interpret this disagreement in the analytical and numerical results as the necessity for replica symmetry breaking [48]. This analysis, however, goes beyond the scope of this paper.

III. DISCUSSION

In this work, we calculated the storage capacity of a quantum perceptron proposed in a recent work [17]. This implementation of a quantum perceptron uses less memory resources compared to its classical counterpart [for N classical spins only $\log_2(N)$ are needed] and has already been implemented on IBM's quantum devices [17,49]. Following the seminal works of Gardner [22,23], we used statistical physics techniques to calculate the storage capacity of this perceptron model. In particular, we interpreted this quantum perceptron as a classical perceptron on an extended input space with a different activation function (see Fig. 1). This interpretation allows us to calculate the storage capacity of a quantum perceptron by computing the relative volume of weights which fulfill a given input-output relation.

To handle the multitude of inputs and learning rules, we integrated the input and the weights. Formally, this averaging over input and weights maps the calculation of the relative volume to the partition function of a classical spin glass problem. Similar to problems in classical spin glass theory, we computed the logarithm of the partition function using the

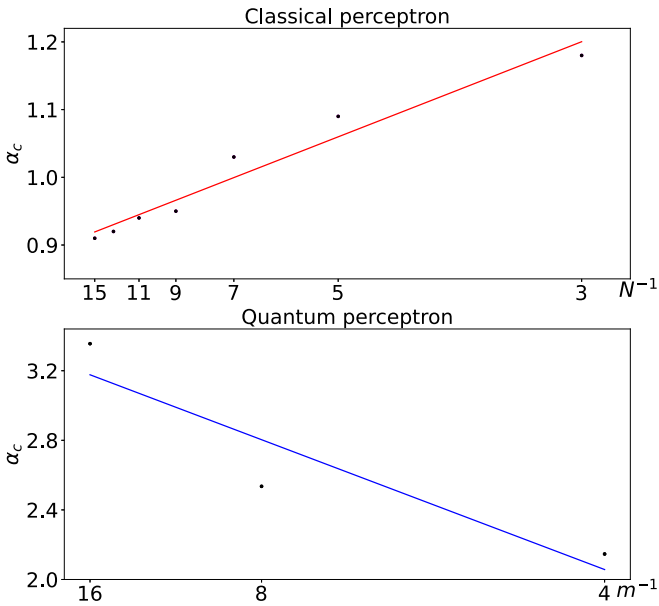


FIG. 3. Storage properties of perceptrons for the Ising weights. Storage capacity for the classical (upper) and quantum (lower) Ising perceptrons as a function of the number of inputs N^{-1} and m^{-1} , respectively. The dots are the result of the Monte Carlo simulations. The intersection of the lines with the y axis gives the storage capacity 0.86 ± 0.01 for the classical and 3.55 ± 0.01 for the quantum perceptron in the limits $N, m \rightarrow \infty$. The error bars can not be seen in this scale.

replica trick [18,30]. Further, by using the large m expansion, we can determine the storage capacity α_c in leading order, which is the ratio of the stored patterns p over the computational resources m . Notably, the techniques presented here are applicable to other quantum architectures.

Given the model of Fig. 1(c), we obtain a maximal critical storage capacity of $\alpha_{c,\max} > 13$ for the spherical weights and Ising inputs (see Fig. 2). To put these results in perspective, we compare them with the classical perceptron. In the classical case, the maximal storage capacity is $\alpha_{c,\max} = 2$ (see Fig. 2). Therefore, the maximum storage capacity of the quantum perceptron is clearly larger than the maximum storage capacity of the classical perceptron. This result agrees with the recent work [50] where the authors found a similar relation to the capacity of quantum neural networks compared to the classical. Even though their definition of capacity is determined by the effective dimension, it also exploits the model's ability to express different relationships between variables.

For Gaussian distributed inputs, the performance of the quantum perceptron is quite different from the classical perceptron following a related work [51]. In the classical case, the relative volume shrinks exponentially with m below the critical capacity, and shrinks suddenly to zero above α_c (see [52]). In this study, the volume shrinks exponentially with m , but the rate of shrinking changes from below (“easy learning” phase) to above α_c (“hard learning” phase). The maximum storage capacity of the “easy learning” phase is 0.125. These results suggest that the performance of quantum perceptron models does not always follow the behavior of their classical

counterparts. Therefore, it emphasizes the need to rigorously study these models and explore their properties as general learning machines.

Another example where contradictory behavior is observed between classical and quantum perceptrons is in the case of Ising weights. The analytical results suggest that $\alpha_{c,\max} = 8/\pi$ while the Monte Carlo simulation suggests that $\alpha_{c,\max} = 3.55 \pm 0.01$. The difference in the slope emphasizes that in the quantum case the maximum storage capacity can be larger than 1 contrary to the classical case. This is because in the classical case the dimension of the input is equal to N , while in the quantum case 2^N . Following the analysis in the classical case, a disagreement between the analytical and numerical result is interpreted as the necessity of replica symmetry breaking in the analytical calculation [18,53]. Thus, the MC solution is more reliable and the analysis on the classical perceptron suggests that the replica symmetry breaking solution needs to be applied for the Ising weights. Therefore, a similar approach might be necessary to tackle the difference between the analytical and numerical result in the quantum case, i.e. by applying replica symmetry breaking. We leave this open for future work.

Moreover, it would be highly important for practical applications to explore the storage properties of the quantum perceptron with correlated inputs or input-output patterns. In a previous analysis of quantum perceptrons [26], one distinguished between three different phases an *ignorant phase*, a *random phase*, and *learning phase*, and it would be interesting to detect these phases in the quantum perceptron architecture of [17]. Future studies should also investigate the storage capacity away from $q \approx 1$ and the dependency on κ . Also, it will be essential to include corrections to the large m expansion and study the stability of the replica symmetric saddle point solution [46]. Finally, an exciting continuation of this work would be to consider other architectures of quantum perceptrons [14,54,55], e.g., qudit based platforms [56–58], and analyze them with the tools presented in this work. Also, it would be interesting to extend the analysis to a network of quantum perceptrons.

This work studied the storage properties of different quantum perceptron models with a direct hardware implementation [17]. Importantly, inspired by the analysis of classical perceptrons [18], we applied statistical physics techniques of spin glasses to the studied quantum models. This also facilitated a certain comparison between the quantum and classical models, even though such a comparison is not perfectly sound. In particular, our work shows and validates that the number of patterns that can be stored in the considered models of quantum perceptrons is exponential in the number of spins N . We defined thus and calculated the corresponding values of the storage capacity for the studied quantum perceptrons as a ratio of the number of patterns p and the total number of spin configurations, $\alpha = p/m = p/2^N$.

IV. METHODS

In this section, we elaborate on the computational details presented in Sec. II, i.e., the averaging over the inputs, the calculation of the effective potential, and the saddle point approximation.

A. Averaging over the input patterns

We perform the average $\langle\langle \cdot \rangle\rangle$ and assume weak correlations between the weights. Then we can approximate

$$\left\langle\left\langle \prod_{\alpha,\mu} e^{-\frac{i}{m} x_\mu^\alpha |\vec{w}^\mu \cdot \vec{w}^\alpha|^2} \right\rangle\right\rangle = e^{-\frac{i}{m} \sum_\alpha x_\mu^\alpha \sum_k (\omega_k^\alpha)} \prod_{\mu,k \neq l} \cos\left(\frac{2}{m} \sum_\alpha x_\mu^\alpha w_k^\alpha w_l^\alpha\right). \quad (29)$$

The above expressions are somewhat similar to those derived in [59], but not the exponential phase factor, effectively shifting the values of λ 's by -1 , and the prefactor $2/m$, multiplying the argument of the $\cos(\cdot)$ function. Using Eq. (29) the relative volume becomes

$$\begin{aligned} \langle\langle V_S \rangle\rangle &= \frac{1}{V_{S_0}^n} \int_w \int_\lambda \int_x \int_E \int_q \int_F \exp\left[i \sum_{\alpha,\mu} x_\mu^\alpha (\lambda_\mu^\alpha - 1) + \sum_{\mu,k,l} \ln \cos\left(\frac{2}{m} \sum_\alpha x_\mu^\alpha w_k^\alpha w_l^\alpha\right) \right] \\ &\times \exp\left[iE^\alpha (|\vec{w}^\alpha|^2 - m) + imF^{\alpha\beta} \left(q^{\alpha\beta} - \frac{1}{m} \sum_k w_k^\alpha w_k^\beta \right) \right]. \end{aligned} \quad (30)$$

Next, we use the approximation $\ln \cos x \approx -x^2/2$ and use Eq. (11). In addition, we employ that the integral

$$I = \int_{-\infty}^{\infty} \prod_{\alpha,\mu} \frac{dx_\mu^\alpha}{2\pi} \int_{\kappa}^{\infty} \prod_{\alpha,\mu} d\lambda_\mu^\alpha \exp\left(i \sum_{\alpha,\mu} x_\mu^\alpha (\lambda_\mu^\alpha - 1) - \sum_{\mu,\alpha} (x_\mu^\alpha)^2 - 2 \sum_{\alpha < \beta, \mu} (q^{\alpha\beta})^2 x_\mu^\alpha x_\mu^\beta \right) \quad (31)$$

factorizes according to

$$I = \left[\int_{-\infty}^{\infty} \prod_{\alpha} \frac{dx^\alpha}{2\pi} \int_{\kappa}^{\infty} \prod_{\alpha} d\lambda^\alpha e^{i \sum_\alpha x^\alpha (\lambda^\alpha - 1) - \sum_\alpha (x^\alpha)^2 - 2 \sum_{\alpha < \beta} (q^{\alpha\beta})^2 x^\alpha x^\beta} \right]^p, \quad (32)$$

which leads to Eqs. (12)–(15).

B. Calculation of G_1

We assume replica symmetry of $q^{\alpha\beta}$ and after the integration over x^μ we have

$$\lim_{n \rightarrow 0} \frac{1}{n} G_1[q] = \int_{-\infty}^{\infty} Dy \ln L(y), \quad (33)$$

where we used the abbreviation (28) and introduce

$$L(y) = 2\sqrt{\pi} \operatorname{Erfc} \left[\frac{\kappa - 1 + yq}{\sqrt{2(1 - q^2)}} \right]. \quad (34)$$

The function $L(y)$ is the main object that distinguishes the classical and the quantum perceptron. In the classical case we have

$$L(y) = 2\sqrt{\pi} \operatorname{Erfc} \left[\frac{\kappa + yq}{\sqrt{(1 - q)}} \right]. \quad (35)$$

In the quantum case, $L(y)$ depends on q^2 since we are dealing with squared scalar products, which leads to an additional factor of 2 in the denominator of $L(y)$; this factor will then be responsible for the increase of the storage capacity for the quantum case in comparison to the classical case.

C. Calculation of G_2 for spherical weights

We also assume replica symmetry of E^α and $F^{\alpha\beta}$ and perform the multidimensional Gaussian integral in Eq. (15) resulting in

$$G_2[E, F] = \ln[(2\pi i)^{n/2} (\det M)^{-1/2}], \quad (36)$$

where we introduced the matrix

$$M^{ab} = (2E + F)\delta^{ab} - F. \quad (37)$$

The matrix M has $n - 1$ degenerate eigenvalues $\Lambda_1 = \dots = \Lambda_{n-1} = 2E + F$ and one nondegenerate eigenvalue $\Lambda_n = 2E - (n - 1)F$ such that the determinant of the matrix M becomes

$$\ln \det M = (n - 1) \ln(2E + F) + \ln[2E - (n - 1)F]. \quad (38)$$

D. Saddle point equations of G for spherical weights

Since G_1 does not depend on E and F the saddle point equations with respect to E and F are

$$0 = \frac{1}{n} \frac{\partial G}{\partial E} = -i + \frac{1}{n} \frac{\partial G_2}{\partial E}, \quad (39a)$$

$$0 = \frac{1}{n} \frac{\partial G}{\partial F} = \frac{i}{2}(n - 1)q + \frac{1}{n} \frac{\partial G_2}{\partial F}, \quad (39b)$$

with

$$\frac{1}{n} \frac{\partial G_2}{\partial E} = \frac{(n - 1)F + 2E(n - 2)}{2(2E + F)(-Fn + 2E + F)}, \quad (40a)$$

$$\frac{1}{n} \frac{\partial G_2}{\partial F} = \frac{(n - 1)F}{2(2E + F)(-Fn + 2E + F)}. \quad (40b)$$

Performing the limit $n \rightarrow 0$ and solving for E and F results in

$$E = \frac{i(1 - 2q)}{2(1 - q)^2}, \quad (41a)$$

$$F = \frac{iq}{(1 - q)^2}. \quad (41b)$$

Further, we define the effective potential

$$g = \lim_{n \rightarrow 0} \frac{1}{n} G \quad (42)$$

and insert the solution of the saddle point equation into G . As a result, we obtain

$$g = \alpha \int_{-\infty}^{\infty} Dy \ln L(y) + \frac{1}{2} \ln(1-q) + \frac{1}{2(1-q)} \quad (43)$$

plus constant terms independent of q . We can interpret the averaged logarithm of the volume g as a kind of free energy (an effective potential), which is a regular function of $0 \leq q < 1$, but has a singularity at $q = 1$. To analyze the role of this singularity, we employ the asymptotic expansion of $\text{Erfc}(x) \approx \sqrt{\pi} x^{-1} e^{-x^2} \theta(x)$ for $x \rightarrow \infty$. We see that

$$g \simeq -\frac{\alpha}{2(1-q)} \int_{1-\kappa}^{\infty} Dy (\kappa - 1 + y)^2 + \frac{1}{2(1-q)} \quad (44)$$

has two singular terms as $q \rightarrow 1$.

We observe that there is here a phase transition. When α is small the term $1/2(1-q)$ is dominant at q going to 1, and ‘‘pushes’’ the minimum of g to zero. For $\alpha > \alpha_c(\kappa)$, where

$$\alpha_c(\kappa) = \left[\int_{1-\kappa}^{\infty} Dy (\kappa - 1 + y)^2 \right]^{-1}, \quad (45)$$

the term with $1/(1-q)$ is negative, and the minimum of g is at $-\infty$ so that in effect the relative volume shrinks to zero. One can check explicitly that $\alpha_c(\kappa)$ is a decreasing function of κ . The free energy at $q = 0$ becomes

$$g(q=0; \kappa) = \alpha \ln \left\{ 2\sqrt{\pi} \text{Erfc} \left[\frac{\kappa - 1}{\sqrt{2}} \right] \right\} + \frac{1}{2}, \quad (46)$$

or after normalization

$$\tilde{g}(q=0) = g(q=0; \kappa) - g(q=0; \kappa=0). \quad (47)$$

We plot the effective potential as a function of α and κ in Fig. 4.

The above analysis implies that the critical value of the storage capacity for $\kappa = 1$, $\alpha_c = 2$. Since $\alpha_c(\kappa)$ grows as κ becomes smaller, performing the integral leads to the maximal critical storage capacity of $\alpha_{c,\max} > 2$ for $\kappa \rightarrow 0$.

E. Calculation of G_1 for Gaussian distributed inputs

First, we define the matrix

$$A_{kk'} = \frac{1}{n} \sum_{\alpha} x^{\alpha} w_k^{\alpha} w_{k'}^{\alpha}, \quad (48)$$

which is spanned by the vectors w^{α} . We can write its non-trivial eigenvectors as combinations of w^{α} . The eigenvalue equation is

$$\frac{1}{n} \sum_{\alpha, k'} x^{\alpha} w_k^{\alpha} w_{k'}^{\alpha} \sum_{\beta} c_{\beta} w_{k'}^{\beta} = \Lambda \sum_{\alpha} c_{\alpha} w_k^{\alpha}. \quad (49)$$

All other eigenvectors of $1 + 2i\hat{A}$ (orthogonal to the vectors w^{α}) are trivial: they correspond to eigenvalues 1 and do not contribute to the $\ln \det$. Comparing coefficients, using the

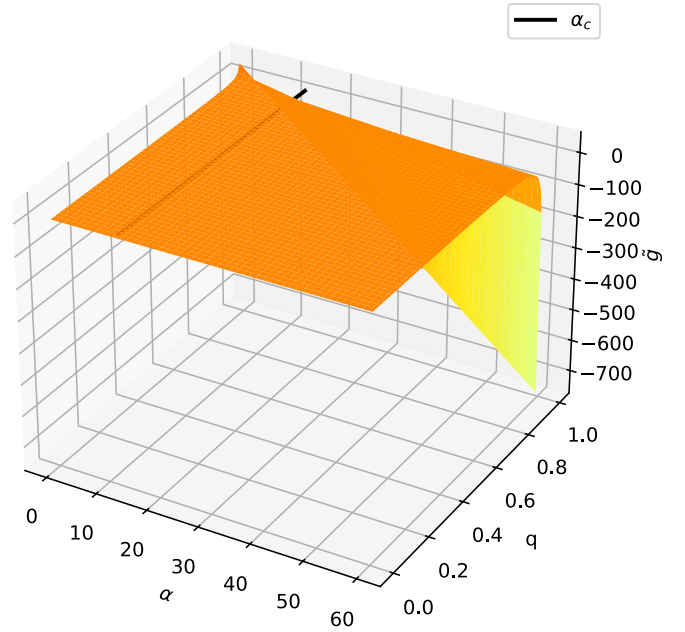


FIG. 4. The effective potential for the spherical weights. We plot the normalized effective potential \tilde{g} of Eq. (47). It changes from finite negative values below α_c to $-\infty$ (represented by the gray area) above α_c . The black line shows the α_c curve given by Eq. (64).

definition of $q^{\alpha\beta}$ and assuming replica symmetry $q^{\alpha\beta} = q$ for $\alpha \neq \beta$, leads to a closed equation

$$1 = \sum_a \frac{x^{\alpha} q}{\Lambda - x^{\alpha}(1-q)} \quad (50)$$

for eigenvalues Λ of \hat{A} . Using the eigenvalues of \hat{A} we can rewrite G_1 as

$$G_1[q] = \ln \int \prod_{\alpha} d\lambda^{\alpha} \int \prod_{\alpha} dx^{\alpha} \frac{\exp(i \sum_{\alpha} x^{\alpha} \lambda^{\alpha})}{\prod_n (1 + 2i\Lambda_n)}. \quad (51)$$

In order to rewrite the product of eigenvalues we transform the self-consistent equation for the eigenvalues Λ into the characteristic polynomial of \hat{A} to define the function

$$W(\Lambda, x) = \prod_{\alpha} [\Lambda - (1-q)x^{\alpha}] - \sum_{\alpha} q x^{\alpha} \prod_{\alpha \neq \beta} [\Lambda - (1-q)x^{\beta}]. \quad (52)$$

Next, we introduce the auxiliary quantity

$$L(\epsilon) = \ln \det(1 + 2i\epsilon \hat{A}) = \sum_n \ln(1 + 2i\epsilon \Lambda_n), \quad (53)$$

where we are interested in the value of $L(1)$. Differentiating with respect to ϵ we obtain

$$\frac{dL}{d\epsilon} = \frac{n}{\epsilon} - \frac{1}{\epsilon} \sum_{\Lambda} \frac{1}{1 + 2i\Lambda\epsilon}. \quad (54)$$

The sum can be rewritten by using Cauchy’s theorem and employing an appropriate contour \mathcal{C} . Using this integral

representation for the sum we obtain

$$\frac{dL}{d\epsilon} = \frac{n}{\epsilon} + \frac{d}{d\epsilon} \ln W(i/(2\epsilon), x). \quad (55)$$

Integrating ϵ from 0 to 1 we get

$$L(1) = \ln W(i/2, x) \quad (56)$$

since $L(\epsilon)$ goes to zero for $\epsilon \rightarrow 0$. Expanding Λ in q , i.e., treating q as a perturbation, G_1 becomes

$$G_1[q] = \ln \int \prod_{\alpha} d\lambda^{\alpha} \int \prod_{\alpha} dx^{\alpha} \exp \left(i \sum_{\alpha} x^{\alpha} \lambda^{\alpha} \right) \times \frac{1}{\prod_{\alpha} \left(\frac{i}{2} - x_{\alpha} \right)} \left[1 + \sum_{\alpha, \beta} \frac{q^2 x^{\alpha} x^{\beta}}{\left(\frac{i}{2} - x_{\alpha} \right) \left(\frac{i}{2} - x_{\beta} \right)} \right]. \quad (57)$$

Performing the integration over x^{α} and λ^{α} gives

$$G_1(q) = -\frac{\kappa n}{2} - \frac{1}{2} n q^2 (2 + \kappa)^2. \quad (58)$$

Due to the perturbative expansion in q the function $G_1(q)$ does not exhibit any singularity at $q = 1$, which will affect the nature of the phase transition, as we will see below.

F. Saddle point equations of g for Gaussian distributed inputs

The effective potential of Eq. (13) becomes

$$g = \alpha \left[-\frac{\kappa}{2} - \frac{1}{2} q^2 (2 + \kappa)^2 \right] + \frac{1}{2} \ln(1 - q) + \frac{1}{2(1 - q)}, \quad (59)$$

plus constant terms independent of q . This function does contain a singular term $(1 - q)^{-1}$, which repulses the saddle point solutions for the minimal value away from $q = 1$. Indeed, taking the derivative of g with respect to q gives

$$\alpha(2 + \kappa)^2 q = \frac{q}{2(1 - q)^2}. \quad (60)$$

This equation has a trivial solution $q = 0$ for which g becomes minimal, and

$$\tilde{g} = g(\kappa) - g(\kappa = 0) = -(\alpha\kappa)/2. \quad (61)$$

This equation has also a nontrivial solution, which exists for $2\alpha(2 + \kappa)^2 \geq 1$. The critical value of the storage capacity is given by (see Appendix D)

$$\alpha_c = \frac{1}{2(2 + \kappa)^2}. \quad (62)$$

Note that the phase transition, in this case, has a different character: for both solutions g , or more importantly \tilde{g} , takes finite negative values, but it changes from $-(\alpha\kappa)/2$ in the “easy to learn” phase to larger negative values in the “hard to learn phase” (see Fig. 5). This behavior might be the result of expansion in q that we used to obtain the effective potential. In the easy to learn phase, the relative volume is 1 at $\kappa = 0$, as expected, but decreases moderately slowly exponentially with m as $\exp(m\tilde{g})$ for nonzero κ . This exponential decrease becomes much faster in the hard to learn phase, as illustrated in Fig. 5. Furthermore, the effective potential might be the first

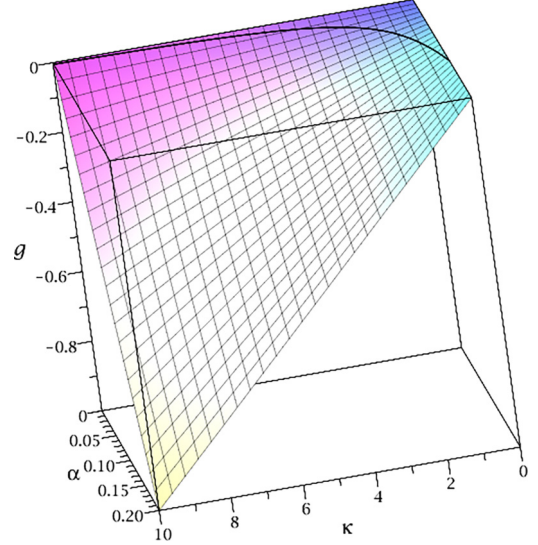


FIG. 5. The effective potential for Gaussian distributed inputs. We plot the effective potential g at the minimum, i.e., at $q = 0$ for $\alpha \leq \alpha_c$, and $q = 1 - \sqrt{1/[2(2 + \kappa)^2\alpha]}$ for $\alpha > \alpha_c$. It changes from small negative values close to zero of Eq. (61) below the α_c curve to larger negative values of Eq. (59) above. The black line shows the α_c curve given by Eq. (62).

term of expansion of $(1 - q^2)^{-1}$ and we discuss this idea in Appendix D, which will bring us back to the volume shrinking phase transition in the manner of Gardner.

G. Calculation of G_2 for Ising weights

Assuming replica symmetry of F^{ab} and averaging over the binary weights, Eq. (26) becomes

$$G_2 = -\frac{1}{2} F n + n \int_{-\infty}^{\infty} Dz \ln[2 \cosh(z\sqrt{F})], \quad (63)$$

as in the classical case [60].

H. Saddle point equations of G for Ising weights

The effective potential with replica symmetry of q^{ab} and F^{ab} becomes

$$g = \alpha \int_{-\infty}^{\infty} Dy \ln L(y) + R(F, q) \quad (64)$$

with

$$R(F, q) = -\frac{1}{2} F(1 - q) + \int_{-\infty}^{\infty} Dz \ln[2 \cosh(z\sqrt{F})]. \quad (65)$$

Then, the saddle point equation with respect to F is

$$-\frac{1}{2}(1 - q) + \int_{-\infty}^{\infty} Dz \frac{z}{2\sqrt{F}} \tanh(z\sqrt{F}) = 0, \quad (66)$$

which is similar to equation obtained for the classical perceptron with binary weights [23], where it was argued that the solution with $F \rightarrow \infty$ as $q \rightarrow 1$ is invalid. Instead, for the correct solution of the classical perceptron problem, replica symmetry breaking must be taken into account.

Here, we analyze results for the replica symmetric case and compare them with Monte Carlo simulations. For the quantum

perceptron, F is a well defined function of q , and it tends to infinity as $q \rightarrow 1$. The last equation can be solved

$$\sqrt{F} \approx \sqrt{\frac{2}{\pi}} \frac{1}{(1-q)}, \quad (67)$$

where $\text{sign}(x) = x/|x|$ and we approximated the tanh by $\text{sign}(x)$.

Comparing the leading terms when $q \rightarrow 1$, we arrive at

$$g \approx \frac{1}{(1-q)} \left[-\frac{\alpha}{4} \int_{-\kappa}^{\infty} Dy(\kappa+y)^2 + \frac{1}{\pi} \right]. \quad (68)$$

In this way we obtain the critical value

$$\alpha_c(\kappa) = \frac{4}{\pi} \left[\int_{-\kappa}^{\infty} Dy(\kappa+y)^2 \right]^{-1}, \quad (69)$$

which implies the maximal value of $\alpha_c(0) = 8/\pi$. In contrast, the MC simulations suggest that $\alpha_c(0) \simeq 3.55$ as illustrated in Fig. 3. As in the classical case, we interpret this discrepancy as the necessity of replica symmetry breaking.

The data that support the findings of this study are available from the corresponding author upon request.

ACKNOWLEDGMENTS

ICFO group acknowledges support from: ERC AdG NOQIA; Grants No. MCIN/AEI PGC2018-0910.13039/501100011033 and No. CEX2019-000910-S/10.13039/501100011033, Plan National FIDEUA Grant No. PID2019-106901GB-I00, Plan National STAMEENA Grant No. PID2022-139099NB-I00, project funded by Grant No. MCIN/AEI/10.13039/501100011033 and by the ‘‘European Union NextGenerationEU/PRTR’’ (Grant No. PRTR-C17.I1), FPI; QUANTERA MAQS Grant No. PCI2019-111828-2); QUANTERA DYNAMITE Grant No. PCI2022-132919 (QuantERA II Programme co-funded by European Union’s Horizon 2020 program under Grant Agreement No. 101017733), Ministry of Economic Affairs and Digital Transformation of the Spanish Government through the QUANTUM ENIA project call–Quantum Spain project, and by the European Union through the Recovery, Transformation, and Resilience Plan–NextGenerationEU within the framework of the Digital Spain 2026 Agenda; Fundació Cellex; Fundació Mir-Puig; Generalitat de Catalunya (European Social Fund FEDER and CERCA program, AGAUR Grant No. 2021 SGR 01452, QuantumCAT Grant No. U16-011424, cofunded by ERDF Operational Program of Catalonia 2014-2020); Barcelona Supercomputing Center MareNostrum (Grant No. FI-2023-1-0013); EU Quantum Flagship (PASQuaS2.1, Grant No. 101113690); EU Horizon 2020 FET-OPEN OPTologic (Grant No 899794); EU Horizon Europe Program (Grant Agreement No. 101080086–NeQST), ICFO Internal ‘‘QuantumGaudi’’ project; European Union’s Horizon 2020 program under the Marie Skłodowska-Curie Grant Agreement No. 847648; ‘‘La Caixa’’ Junior Leaders fellowships, La Caixa’’ Foundation (ID 100010434); Grant No. CF/BQ/PR23/11980043. Views and opinions expressed are, however, those of the author(s) only and do not necessarily reflect those of the European Union,

European Commission, European Climate, Infrastructure and Environment Executive Agency (CINEA), or any other granting authority. Neither the European Union nor any granting authority can be held responsible for them.

All authors contributed to the design and implementation of the research, to the analysis of the results, and to the writing of the manuscript.

The authors declare no competing financial or nonfinancial interests.

APPENDIX A: DETAILS ON THE QUANTUM PERCEPTRON PROPOSED IN [17]

The first unitary $U_{\vec{i}}$ should fulfill

$$|\psi_{\vec{i}}\rangle = U_{\vec{i}}|0\rangle^{\otimes N}, \quad (A1)$$

and in this way encodes the information on N qubits. Particularly, any $m \times m$ unitary matrix with the first column being identical with \vec{i} and normalized is a valid candidate for such a unitary. The information is processed by applying the second unitary $V_{\vec{w}}$ which fulfills

$$V_{\vec{w}}|\psi_{\vec{i}}\rangle = |1\rangle^{\otimes N} = |m-1\rangle. \quad (A2)$$

Applying the unitary $V_{\vec{w}}$ on the encoded state leads to

$$|\phi_{\vec{i},\vec{w}}\rangle \equiv V_{\vec{w}}|\psi_{\vec{i}}\rangle = \sum_{j=0}^{m-1} c_j|j\rangle. \quad (A3)$$

Performing multi-controlled-NOT gates with a readout qubit leads to the state

$$|\phi_{i,w}\rangle|0\rangle = \sum_{j=0}^{m-2} c_j|j\rangle|0\rangle + c_{m-1}|m-1\rangle|1\rangle. \quad (A4)$$

As a result, when measuring 1 on the readout qubit, the probability amplitude is

$$|c_{m-1}|^2 = |\vec{i}^\mu \cdot \vec{w}|^2. \quad (A5)$$

APPENDIX B: ABBREVIATIONS

In this Appendix, we summarize the abbreviation used in the main text. In Eqs. (5) and (6) we used

$$\int_w = \int_{-\infty}^{\infty} \prod_k dw_k, \quad (B1)$$

and in Eq. (9) the measure is

$$\begin{aligned} \int_w \int_\lambda \int_x \int_E &= \int_{-\infty}^{\infty} \prod_k dw_k \int_\kappa \prod_\mu d\lambda^\mu \\ &\times \int_{-\infty}^{\infty} \prod_\mu \frac{dx^\mu}{2\pi} \int_{-\infty}^{\infty} \frac{dE}{2\pi}, \end{aligned} \quad (B2)$$

in Eq. (12) the abbreviation means

$$\int_F \int_q \int_E = \int_{-\infty}^{\infty} \prod_{\alpha < \beta} dq^{\alpha\beta} \int_{-\infty}^{\infty} \prod_{\alpha < \beta} \frac{dF^{\alpha\beta}}{2\pi} \int_{-\infty}^{\infty} \prod_\alpha \frac{dE^\alpha}{2\pi}, \quad (B3)$$

and in Eq. (30) we used

$$\begin{aligned} & \int_w \int_\lambda \int_x \int_E \int_q \int_F \\ &= \int_{-\infty}^{\infty} \prod_{k,\alpha} dw_k^\alpha \int_{\kappa} \prod_{\mu,\alpha} d\lambda_\mu^\alpha \int_{-\infty}^{\infty} \prod_{\alpha,\mu} \frac{dx_\mu^\alpha}{2\pi} \\ & \times \int_{-\infty}^{\infty} \prod_{\alpha} \frac{dE^\alpha}{2\pi} \int_{-\infty}^{\infty} \prod_{\alpha<\beta} dq^{\alpha\beta} \int_{-\infty}^{\infty} \prod_{\alpha<\beta} \frac{dF^{\alpha\beta}}{2\pi}. \quad (\text{B4}) \end{aligned}$$

APPENDIX C: MONTE CARLO SIMULATION

We apply the Monte Carlo simulation of the classical perceptron with Ising weights [53] to the quantum perceptron. Here, we elaborate the details of the Monte Carlo simulation.

The first pattern $i_1^\mu = \pm 1$ is chosen at random and we fix a certain threshold κ . Then, we go through all possible realizations of the weights and keep only the weights that satisfy the given threshold κ . This forms the remaining set of the weights, i.e., the weights that satisfy the given patterns. Then, a second pattern is chosen at random and we go through all possible realizations of the remaining set of the weights to keep again only the subset of weights which satisfy the given threshold κ . Then, we continue by choosing more random patterns and updating the set of the weights that fulfill the given threshold. After a certain number of P patterns that have been introduced to the perceptron, no choice for the weights exist for $P + 1$ patterns. This means that for this sample the system can store exactly P patterns.

Therefore, the value of P depends on the random choices of the $\sum_k i_k^\mu = \pm 1$ and the threshold κ . The threshold κ in both cases is taken to be zero. We need to average P over many samples and define the estimate of the storage capacity for a system of size N_s :

$$\alpha(N_s) = \frac{\langle P \rangle}{N_s}. \quad (\text{C1})$$

For the numerical simulations in Fig. 3, N_s is equal to N and m for the classical and quantum perceptron, respectively. Moreover, we have 2^N and 2^m realizations of the weights for the classical and quantum models, respectively. We used 10 000 samples for each simulation and we performed them three times to estimate the error. In Fig. 3, we choose odd values of N to always have ± 1 for the classical output and we use $m = 4, 8, 16$ since for larger m the computation becomes intractable.

APPENDIX D: SPECULATIONS ABOUT THE GAUSSIAN INPUTS

In the derivation of the basic expression

$$g = \alpha \left[-\frac{\kappa}{2} - \frac{1}{2} q^2 (2 + \kappa)^2 \right] + \frac{1}{2} \ln(1 - q) + \frac{1}{2(1 - q)}, \quad (\text{D1})$$

where we used an expansion in q , eliminating a part of the singular behavior at $q \rightarrow 1$. The next order contribution in the effective potential is presumably

$$\begin{aligned} & \left[-\frac{\kappa}{2} - \frac{1}{2} q^2 (2 + \kappa)^2 \right] \\ & \approx \left[-\frac{\kappa}{2} + \frac{1}{2} (2 + \kappa)^2 - \frac{1}{2(1 - q^2)} (2 + \kappa)^2 \right] \end{aligned}$$

and suggests that

$$\alpha_c (2 + \kappa)^2 / 2 = 1,$$

implying maximal $\alpha_c(\kappa = 0) = \frac{1}{2}$.

-
- [1] M. van Gerven and S. Bohte, *Front. Comput. Neurosci.* **11**, 114 (2017).
 - [2] G. Carleo, I. Cirac, K. Cranmer, L. Daudet, M. Schuld, N. Tishby, L. Vogt-Maranto, and L. Zdeborová, *Rev. Mod. Phys.* **91**, 045002 (2019).
 - [3] S. Angra and S. Ahuja, in *2017 International Conference on Big Data Analytics and Computational Intelligence (ICBDAC)* (IEEE, Piscataway, NJ, 2017), pp. 57–60.
 - [4] J. Schmidhuber, *Neural Networks* **61**, 85 (2015).
 - [5] F. Rosenblatt, *Psychol. Rev.* **65**, 386 (1958).
 - [6] M. Minsky and S. Papert, *Perceptrons: An Introduction to Computational Geometry* (MIT Press, Cambridge, MA, 1969).
 - [7] J. VanderPlas, A. J. Connolly, Z. Ivezic, and A. Gray, in *2012 Conference on Intelligent Data Understanding* (IEEE, Piscataway, NJ, 2012), pp. 47–54.
 - [8] A. N. Michel and J. A. Farrell, *IEEE Control Syst. Mag.* **10**, 6 (1990).
 - [9] E. Ikonomakis, S. Kotsiantis, and V. Tampakas, *WSEAS Trans. Comput.* **4**, 966 (2005).
 - [10] B. Aubin, W. Perkins, and L. Zdeborová, *J. Phys. A: Math. Theor.* **52**, 294003 (2019).
 - [11] J. Fraxanet, T. Salamon, and M. Lewenstein, The coming decades of quantum simulation, in *Sketches of Physics: The Celebration Collection*, edited by R. Citro, M. Lewenstein, A. Rubio, W. P. Schleich, J. D. Wells, and G. P. Zank (Springer International Publishing, Cham, 2023), pp. 85–125.
 - [12] M. Schuld, I. Sinayskiy, and F. Petruccione, *Quantum Inf. Process.* **13**, 2567 (2014).
 - [13] H.-Y. Huang, M. Broughton, M. Mohseni, R. Babbush, S. Boixo, H. Neven, and J. R. McClean, *Nat. Commun.* **12**, 2631 (2021).
 - [14] M. Schuld, I. Sinayskiy, and F. Petruccione, *Phys. Lett. A* **379**, 660 (2015).
 - [15] P. Torta, G. B. Mbeng, C. Baldassi, R. Zecchina, and G. E. Santoro, *arXiv:2112.10219*.
 - [16] N. Wiebe, A. Kapoor, and K. M. Svore, *arXiv:1602.04799*.
 - [17] F. Tacchino, C. Macchiavello, D. Gerace, and D. Bajoni, *npj Quantum Inf.* **5**, 26 (2019).

- [18] H. Nishimori, *Statistical Physics of Spin Glasses and Information Processing* (Oxford University Press, Oxford, 2001).
- [19] J. Hopfield, *Proc. Natl. Acad. Sci. USA* **79**, 2554 (1982).
- [20] D. Amit, *Modelling Brain Function* (Cambridge University Press, Cambridge, 1989).
- [21] N. Davey and R. Adams, *Connect. Sci.* **16**, 47 (2004).
- [22] E. Gardner, *J. Phys. A: Math. Gen.* **21**, 257 (1988).
- [23] E. Gardner and B. Derrida, *J. Phys. A: Math. Gen.* **21**, 271 (1988).
- [24] M. G. Díaz, G. Sentís, R. Muñoz-Tapia, and A. Sanpera, *Phys. Rev. Res.* **4**(2), 023228 (2022).
- [25] K. Życzkowski, P. Horodecki, A. Sanpera, and M. Lewenstein, *Phys. Rev. A* **58**, 883 (1998).
- [26] M. Lewenstein, *J. Mod. Opt.* **41**, 2491 (1994).
- [27] M. Lewenstein, A. Gratsea, A. Riera-Campeny, A. Aloy, V. Kasper, and A. Sanpera, *Quantum Sci. Technol.* **6**, 045002 (2021).
- [28] C. Artiago, F. Balducci, G. Parisi, and A. Scardicchio, *Phys. Rev. A* **103**, L040203 (2021).
- [29] M. Schuld and N. Killoran, *Phys. Rev. X Quantum* **3**, 030101 (2022).
- [30] B. Müller, J. Reinhardt, and M. T. Strickland, *Neural Networks, Physics of Neural Networks* (Springer, Berlin, 1995).
- [31] F. Fan, W. Cong, and G. Wang, [arXiv:1807.03215](https://arxiv.org/abs/1807.03215).
- [32] F. Fan, H. Shan, M. K. Kalra, R. Singh, G. Qian, M. Getzin, Y. Teng, J. Hahn, and G. Wang, *IEEE Trans. Med. Imaging* **39**, 2035 (2020).
- [33] M. Andreucut and M. K. Ali, *Int. J. Mod. Phys. B* **17**, 2447 (2003).
- [34] D. Ventura and T. Martinez, *Inf. Sci.* **124**, 273 (2000).
- [35] L. G. Wright and P. L. McMahon, in *Conference on Lasers and Electro-Optics* (OSA, Washington, DC, 2020), p. JM4G.5.
- [36] A. Pozas-Kerstjens, G. Muñoz-Gil, E. Piñol, M. Á. García-March, A. Acín, M. Lewenstein, and P. R. Grzybowski, *Mach. Learn.: Sci. Technol.* **2**, 025026 (2021).
- [37] H. Ramsauer, B. Schaffl, J. Lehner, P. Seidl, M. Widrich, L. Gruber, M. Holzleitner, M. Pavlović, G. K. F. Sandve, V. Greiff, D. P. Kreil, M. Kopp, G. Klambauer, J. Brandstetter, and S. Hochreiter, [arXiv:2008.02217](https://arxiv.org/abs/2008.02217).
- [38] D. Krotov and J. J. Hopfield, in *Advances in Neural Information Processing Systems*, edited by D. Lee, M. Sugiyama, U. Luxburg, I. Guyon, and R. Garnett, Vol. 29 (Curran Associates, Inc., Red Hook, NY, 2016).
- [39] D. Krotov and J. J. Hopfield, [arXiv:2008.06996](https://arxiv.org/abs/2008.06996).
- [40] C. Lucibello and M. Mézard, *Phys. Rev. Lett.* **132**, 077301 (2024).
- [41] M. Demircigil, J. Heusel, M. Löwe, S. Uppgang, and F. Vermet, *J. Stat. Phys.* **168**, 288 (2017).
- [42] H. Sompolinsky, in *Heidelberg Colloquium on Glassy Dynamics*, edited by J. L. van Hemmen and I. Morgenstern (Springer, Berlin, 1987), pp. 485–527.
- [43] M. Minsky and S. Papert, *Perceptrons: An Introduction to Computational Geometry* (The MIT Press, Cambridge, MA, 1972).
- [44] T. M. Cover, *IEEE Trans. Electron. Comput.*, **EC-14**, 326 (1965).
- [45] D. Sherrington and S. Kirkpatrick, *Phys. Rev. Lett.* **35**, 1792 (1975).
- [46] M. Mézard, G. Parisi, and M. Virasoro, *Spin Glass Theory and Beyond* (World Scientific, Singapore, 1986).
- [47] G. Parisi, *J. Phys. A: Math. Gen.* **13**, L115 (1980).
- [48] G. Parisi, [arXiv:cond-mat/0205387](https://arxiv.org/abs/cond-mat/0205387).
- [49] S. Mangini, F. Tacchino, D. Gerace, C. Macchiavello, and D. Bajoni, *Mach. Learn.: Sci. Technol.* **1**, 045008 (2020).
- [50] A. Abbas, D. Sutter, C. Zoufal, A. Lucchi, A. Figalli, and S. Woerner, *Nat. Comput. Sci.* **1**, 403 (2021).
- [51] F. Benatti, G. Gramegna, and S. Mancini, *J. Phys. A: Math. Theor.* **55**, 155301 (2022).
- [52] J. F. Fontanari and R. Meir, *J. Phys. A: Math. Gen.* **22**, L803 (1989).
- [53] E. Gardner and B. Derrida, *J. Phys. A: Math. Gen.* **22**, 1983 (1989).
- [54] E. Torrontegui and J. J. García-Ripoll, *Europhys. Lett.* **125**, 30004 (2019).
- [55] A. Gratsea and P. Huembeli, [arXiv:2105.01477](https://arxiv.org/abs/2105.01477).
- [56] V. Kasper, D. González-Cuadra, A. Hegde, A. Xia, A. Dauphin, F. Huber, E. Tiemann, M. Lewenstein, F. Jendrzejewski, and P. Hauke, *Quantum Sci. Technol.* **7**, 015008 (2022).
- [57] J. R. Weggemans, A. Urech, A. Rausch, R. Spreeuw, R. Boucherie, F. Schreck, K. Schoutens, J. Minář, and F. Speelman, *Quantum* **6**, 687 (2022).
- [58] M. Ringbauer, M. Meth, L. Postler, R. Stricker, R. Blatt, P. Schindler, and T. Monz, *Nat. Phys.* **18**, 1053 (2022).
- [59] G. Kohring, *J. Phys. France* **51**, 145 (1990).
- [60] W. Krauth and M. Mézard, *J. Phys. France* **50**, 3057 (1989).